NASA TECHNICAL NOTE

NASA TN D-3193

NASA TN D-3193

EXPERIMENTAL STABILITY AND DRAG OF A POINTED AND A BLUNTED 30° HALF-ANGLE CONE AT MACH NUMBERS FROM 11.5 TO 34 IN AIR

by Peter F. Intrieri

Ames Research Center
Moffett Field, Calif.

NATIONAL AERONAUTICS AND SPACE ADMINISTRATION • WASHINGTON, D. C. • JANUARY 1966

EXPERIMENTAL STABILITY AND DRAG OF A POINTED AND A BLUNTED 30° HALF-ANGLE CONE AT MACH NUMBERS FROM 11.5 TO 34 IN AIR

By Peter F. Intrieri

Ames Research Center
Moffett Field, Calif.

NATIONAL AERONAUTICS AND SPACE ADMINISTRATION

For sale by the Clearinghouse for Federal Scientific and Technical Information
Springfield, Virginia 22151 – Price $2.00

EXPERIMENTAL STABILITY AND DRAG OF A POINTED AND A BLUNTED 30° HALF-ANGLE CONE AT MACH NUMBERS FROM 11.5 TO 34 IN AIR

By Peter F. Intrieri
Ames Research Center

SUMMARY

An experimental study has been conducted of the static and dynamic stability and drag characteristics of a pointed and a spherically blunted 30° half-angle cone in air at velocities of about 4 km/sec, 6.7 km/sec, and 8.5 km/sec, corresponding to nominal Mach numbers of 11.5, 19.5, and 34, respectively, and at Reynolds numbers from about 80,000 to 170,000 based on model base diameter. For center-of-gravity locations representative of solid homogeneous models, both configurations were statically stable at all Mach numbers throughout the angle-of-attack range of the investigation. The static stability of the pointed cone increased somewhat with increasing Mach number. The static stability of the blunted cone was essentially invariant with Mach number and greater than that of the pointed cone by as much as 40 percent. The static stability of both configurations decreased with increasing angle of attack. The nonlinear variations of pitching moment with angle of attack for both configurations were closely approximated by a cubic polynomial. Both configurations were dynamically stable at Mach numbers of 11.5 and 19.5 for unpowered flight at constant altitude and exhibited pitching motions which converged at the rate of about 3 percent per cycle. At a Mach number of 34 the blunted cone exhibited increased dynamic stability; the pointed cone exhibited dynamic instability. The dynamic instability of the pointed cone became less severe with increasing angle of attack. The drag coefficient of both configurations increased with increasing angle of attack and remained essentially constant with increasing Mach number. The drag of the blunted cone was approximately 8 percent greater than that of the pointed cone.

The static stability and drag characteristics of both configurations were predicted by Newtonian theory and, for the pointed cone, by conical-flow theory, usually within about 10 percent. Estimates of the dynamic stability of both configurations calculated using Newtonian theory were in agreement with the experimental results at Mach numbers of 11.5 and 19.5.

INTRODUCTION

For entries into planetary atmospheres at velocities well in excess of earth-escape velocity, references 1 and 2 have demonstrated the desirability of using pointed, conical entry bodies to reduce the total aerodynamic heating. Radiative heating, which is much greater than convective heating for very blunt configurations at these very high speeds, depends on the velocity normal to the bow shock wave rather than on the free-stream velocity and, therefore, can be

drastically reduced by using entry bodies with highly swept bow shock waves. References 1 and 2 show that the total aerodynamic heating for entry above the escape speed into the earth's atmosphere (ref. 1) and the atmosphere of Venus (ref. 2) will be minimum for a cone half-angle of about 30°.

The design of an entry vehicle also requires knowledge of the static and dynamic stability and drag characteristics to determine whether these characteristics are adequate to orient the heat shield properly during the entry and to prevent divergent oscillations from occurring at altitudes below that for maximum dynamic pressure. Since pointed entry bodies may undergo a significant amount of nose blunting due to ablation during entry, it is important to determine the effect of this change in nose bluntness on the stability characteristics.

Some experimental data are available on the static stability and drag characteristics of the pointed 30° half-angle cone (see, e.g., refs. 3-6). However, with the exception of reference 5, which presents the static and the dynamic stability and drag of a pointed 30° half-angle cone with afterbody in air (and also in an N_2-CO_2 mixture) at Mach numbers up to 13.5, the only experimental stability data available above a Mach number of 8 were obtained in helium at a Mach number of 20.3 (see ref. 6).

The purpose of this investigation was to determine the static and dynamic stability and drag characteristics of a pointed and a moderately blunted 30° half-angle cone in air at hypersonic Mach numbers to about 30. The investigation was conducted in the prototype of the Ames Hypervelocity Free-Flight Facility in air. The model velocities were 4 km/sec, 6.7 km/sec, and 8.5 km/sec, corresponding to nominal Mach numbers of 11.5, 19.5, and 34, respectively. The free-stream Reynolds numbers ranged from 80,000 to 170,000, based on model base diameter. The present experimental results are compared with other available experimental data and also with estimates made using Newtonian theory and conical-flow theory.

SYMBOLS

A reference area, model base area, m^2

C_D drag coefficient, $\frac{\text{total drag}}{q_\infty A}$

C_{D_o} drag coefficient at zero angle of attack

C_L lift coefficient, $\frac{\text{lift force}}{q_\infty A}$

C_{L_α} lift-curve slope, $\frac{dC_L}{d\alpha}$, per radian

C_m pitching-moment coefficient, $\frac{\text{pitching moment}}{q_\infty A d}$

C_{m_α}	pitching-moment-curve slope, $\frac{dC_m}{d\alpha}$, per radian
$C_{m_{\alpha_L}}$	pitching-moment-curve slope based on a frequency-equivalent linear pitching-moment curve, per radian
$C_{m_q} + C_{m_{\dot{\alpha}}}$	damping-in-pitch derivative $\frac{\partial C_m}{\partial(qd/V_\infty)} + \frac{\partial C_m}{\partial(\dot{\alpha}d/V_\infty)}$, per radian
d	reference diameter, model base diameter, cm
I_y	moment of inertia about a transverse axis through the center of gravity, kg-m^2
k	transverse radius of gyration, m
k_1	constant in equation (1)
K_1, K_2, K_3	constants in equation (2), deg
m	mass of model, g
M_∞	free-stream Mach number
M_a	Mach number of countercurrent air stream
p	roll parameter, $\frac{\text{roll rate}}{\text{velocity}}$, radians/m
q	angular pitching velocity, radians/sec
q_∞	free-stream dynamic pressure, N/m^2
r_n	nose radius of curvature, cm
Re	Reynolds number based on free-stream air properties and model base diameter
T_∞	free-stream air temperature, ^oK
V_∞	free-stream velocity, km/sec
V_a	velocity of countercurrent air stream in laboratory coordinates, km/sec
x	distance along flight path relative to the free-stream air, m
x_{cg}	axial distance from model base to center-of-gravity position, cm
y	horizontal coordinate normal to the flight path, m
z	coordinate normal to the flight path and y axis, m

α angle of attack (angle between model axis and resultant wind direction projected onto the vertical plane), deg

β angle of sideslip (angle between model axis and resultant wind direction projected onto the horizontal plane), deg

$\eta_{1,2}$ damping parameters in equation (2), per m

θ,ψ attitude coordinates of the model relative to earth-fixed axes, deg

λ wave length of pitching oscillation, m/cycle

ξ dynamic-stability parameter for constant altitude (eq. (5))

ρ_∞ free-stream air density, kg/m^3

ρ_o standard sea-level air density, 1.225 kg/m^3

σ resultant angle of attack, $\tan^{-1}\sqrt{\tan^2\alpha + \tan^2\beta}$, deg

σ_m maximum resultant angle of attack, deg

σ_o minimum resultant angle of attack, deg

σ_{rms} root-mean-square resultant angle of attack, $\sqrt{\frac{\int_o^x \sigma^2\,dx}{x}}$, deg

ω_1,ω_2 rate of rotation of complex vectors which generate the model pitching motion (eq. (2)), radians/m

$(\dot{})$ first derivative with respect to time

Subscripts

f final value

i initial value

max maximum

DESCRIPTION OF TESTS

Test Technique and Test Conditions

The tests were performed in the prototype of the Ames Hypervelocity Free-Flight Facility by launching models from a light-gas gun into either still air or into a countercurrent air stream. The countercurrent air stream of 1.8 km/sec was generated by a shock-tube-driven hypersonic nozzle which is contoured to provide flow at a Mach number of 7. The reservoir air for this facility is heated in a cold helium-driven shock tube which is operated under

tailored interface conditions. Figure 1 is a schematic view of the facility. A detailed description of the facility and its operating cycle may be found in reference 7. The light-gas gun was similar to the one described in reference 8. It had a deformable piston and a 12.7-mm bore. The models were launched at nominal velocities of 4 km/sec and 6.7 km/sec into still air at ambient temperature corresponding to nominal Mach numbers of 11.5 and 19.5, respectively; at 6.7 km/sec (the same model velocity used in the $M_\infty = 19.5$ tests) they were launched into the 1.8 km/sec countercurrent air stream to give a combined velocity of about 8.5 km/sec. At the ambient temperature of the test stream, this velocity corresponds to a nominal Mach number of 34. In order to obtain adequate definition of the motions of the models in the test section with the given spacing of the observation stations (see below), the tests were conducted at reduced free-stream densities, ρ_∞/ρ_o of about 0.02, to give the desired wave length of oscillation. Free-stream properties for the tests into still air were determined from measurements of the pressure and temperature in the test section immediately prior to launching the model. These measurements of pressure and temperature gave free-stream density within 2.5 percent for the tests in still air. When the facility is operated with its countercurrent air stream, the free-stream properties are determined by the following procedure. The stream total enthalpy (relative to the laboratory) is determined from measurements of the initial charging pressures and temperatures, velocity of the incident shock, and transient history of stagnation-region pressures in the shock tube. The test-section free-stream velocity and density are then determined from measurements of the static pressure at various stations in the test section, assuming isentropic flow. Calibration measurements of pitot pressure and Mach number (the latter determined from measurements of the shock-wave angle on a stationary cone) have shown that the described density determinations are accurate to within 10 percent. For the present tests, analysis of the pressure records obtained at the various stations in the test section during the model flights indicated a steady decrease in free-stream density of about 10 to 20 percent from the beginning to the end of each of the recorded flight trajectories of the models. The average free-stream density determined from these straight-line variations of density with distance (or time) for each independent flight of the model was used to compute the stability and drag coefficients at this Mach number ($M_\infty = 34$). The drag data (to be presented later) suggest that the free-stream density at Mach number 34 may be approximately 6 percent higher than the average value used in the computations if drag coefficient is actually constant with increasing Mach number from 11.5 to 34. The gradient in free-stream density, it was determined, had little effect on the drag and static-stability coefficients (although these coefficients are still accurate to only ±10 percent due to the initial uncertainty in determining free-stream density as stated above); its effect on the dynamic-stability results is discussed in that section of the report. The average values of Mach number, velocity, and Reynolds number are listed in table I for each flight. The nominal test conditions are summarized below.

SUMMARY OF NOMINAL TEST CONDITIONS

M_∞	V_∞, km/sec	Test environment	ρ_∞, kg/m^3	T_∞, $^\circ K$
11.5	4.0	Still air	$0.033(6.5\times10^{-5}$ slug/ft^3)	295
19.5	6.7	Still air	$.033(6.5\times10^{-5}$ slug/ft^3)	295
34.0	8.5	Countercurrent air stream $M_a \approx 7$, $V_a \approx 1.8$ km/sec	$.021(4.0\times10^{-5}$ slug/ft^3)	170

The trajectory of the model through the test section was recorded by 11 spark shadowgraph stations located at about 1.2-meter intervals. An enlarged view of part of the test section is shown in the inset to figure 1. Side and top views of the models were recorded at each station. The shadowgraphs contained images of reference wires from which x, y, z, θ, and ψ coordinates were read. The linear coordinates were measured to within 0.007 cm, and the angles, to within 0.5°. The orientation angles, θ and ψ, were read relative to earth-fixed axes. No corrections were made for the angle between the resultant wind direction and earth-fixed axes to yield α and β since for these tests these corrections were within the reading accuracy of the angles θ and ψ. Time of model flight between stations was recorded with electronic chronographs to within 0.02 μsec.

Models and Sabots

Sketches of the models used in the present investigation showing pertinent nominal dimensions are presented in figure 2. The models were solid homogeneous bodies machined from either 7075-T6 aluminum or Teflon. The aluminum models were tested at a Mach number of 11.5. At the higher Mach numbers (M_∞ = 19.5 and 34) the heating rates encountered were sufficiently high to cause the metal models to burn in flight. The models in the high-speed tests were made of Teflon, which was found to be a successful heat shield. The Teflon ablated during the flights but the changes in shape, particularly blunting of the tip, were observed in the shadowgraphs to be insignificant. It should be mentioned that each aluminum model had a small shaft extending from the base to facilitate reading the model's position in the shadowgraph pictures. It was not possible to use similar shafts on the Teflon models since these plastic shafts were usually sheared off during the launching process. The dimensions and mass of each model were measured to within ±0.0005 cm (0.1 percent d) and ±0.0002 g (0.1 percent), respectively. Because the models were small and of low mass, measurement of the center-of-gravity position and moment of inertia of the models by existing techniques was not practical; therefore, computed values were used. Since the dimensions of the models varied only slightly from those shown in figure 2, these nominal dimensions were used in the computations. The actual center-of-gravity position of the models is estimated to be within ±0.0025 cm of the computed values. Some of the physical characteristics of each model are listed in table I.

Photographs of the models and sabots are presented in figure 3. The aluminum models were launched by means of the two-piece sabot shown in figure 3(a). The Teflon models failed when launched with this sabot but were launched successfully by means of the sabot shown in figure 3(b). Each sabot was machined from Lexan (polycarbonate plastic) and upon leaving the gun was separated from the model by aerodynamic forces acting on the front face.

REDUCTION OF DATA

Drag

Drag coefficients were determined from the time-distance data of each flight by the method presented in reference 9, which assumes a constant drag coefficient. A method applicable to cases where the drag coefficient varies with angle of attack is presented in reference 10. It is shown in this reference that if the drag coefficient varies with the square of the local resultant angle of attack, according to the relation

$$C_D = C_{D_o} + k_1\sigma^2 \tag{1}$$

the effective constant drag coefficient obtained by the method of reference 9 is the drag coefficient that would be obtained at a constant angular displacement equal to the root-mean-square resultant angle of attack, σ_{rms}, determined from the angular orientation-distance history of each flight. The present results were found to be adequately represented by equation (1) and are therefore correlated with σ_{rms}.

Stability Derivatives

The stability derivatives were determined from analysis of the pitching and yawing motions experienced by the models during free flight. Examples of the types of motions encountered in the present tests, as viewed in the α-β plane, are shown in figure 4. The angles of attack and sideslip measured from the shadowgraphs at each station are indicated by the symbols. The curves show the theoretical motions which best fit the experimental data, and they were computed by a method discussed later in this section. The models in these tests were axially symmetric so that the angular displacement of the model, at any instant, can be represented also by the resultant angle of attack, σ, whose orthogonal components are the angles α and β. As indicated by the representative examples presented in figure 4, the motions obtained for both configurations at all Mach numbers were characterized by relatively narrow, precessing ellipses (in the α-β plane), and the angle-of-attack range through which the models oscillated differed for each flight. Also it is important to point out in figure 4 that the models underwent between 1-1/2 and 2 cycles of oscillation during flight through the instrumented test section, which is sufficient for determining static stability and usually adequate for determining dynamic stability although more cycles of well-defined motion will generally produce better dynamic-stability results.

The analysis of the pitching and yawing motions of the models, to obtain the stability coefficients, consisted in fitting the following equation to the measurements of α and β of each flight

$$\beta + i\alpha = K_1 e^{(\eta_1 - i\omega_1)x} + K_2 e^{(\eta_2 - i\omega_2)x} + K_3 e^{ipx} \tag{2}$$

where $\eta_{1,2}$ and $\omega_{1,2}$ are functions of the aerodynamic stability coefficients and $K_{1,2,3}$ are functions of the initial conditions. Equation (2) is the solution to the differential equation of motion in α and β (including effects of small amounts of roll rate and trim), as given in reference 11, and is based on the assumption of a linear variation of restoring moment with angle of attack. The development of equation (2) also assumes a symmetrical configuration and small angular displacements. Equation (2), programmed for machine computation, was used to select optimum values of the constants by an iterative process of differential corrections.

The curves presented in figure 4 show the theoretical motions obtained by fitting equation (2) to the experimental data. The closeness of the theoretical motions to the experimental data is a measure of the reliability of the stability results. The fitted curves for all flights analyzed in this investigation agreed with the measured angles within the measuring accuracy.

The static-stability derivative, $C_{m_{\alpha_L}}$, based on a linear moment curve, was computed from the wave length of oscillation using the relation

$$C_{m_{\alpha_L}} = -\frac{8\pi^2 I_y}{\lambda^2 \rho_\infty A d} \tag{3}$$

where

$$\lambda = \frac{2\pi}{\sqrt{\omega_1 \omega_2}} \tag{4}$$

and ω_1 and ω_2 are determined from equation (2).

The dynamic-stability parameter, ξ, defined as

$$\xi = C_D - C_{I_\alpha} + (C_{m_q} + C_{m_{\dot{\alpha}}})\left(\frac{d}{k}\right)^2 \tag{5}$$

was determined from the constants η_1 and η_2 by means of the relation

$$\eta_1 + \eta_2 = \frac{\rho_\infty A}{2m}\,\xi \tag{6}$$

It has been shown in references 3 and 12 that ξ, in the form shown in equation (5), is a convenient parameter for describing the dynamic stability of a vehicle in unpowered free flight at constant altitude and in ballistic entry, respectively. The values of ξ, presented in this report, were obtained from equations (2) and (6), which assume a linear system over the angle-of-attack

range covered during any one flight. Each value of ξ, therefore, is the dynamic-stability parameter of an equivalent linear system whose amplitude of oscillation would grow or diminish in the same way as that experienced by the model.

RESULTS AND DISCUSSION

The experimental results of this investigation are summarized in table I, where the measured values of C_D, $C_{m_{\alpha_L}}$, and ξ, based on model base diameter and frontal area, are listed for each flight. Values of σ_m, σ_o, and σ_{rms} are also presented in table I to indicate the angle-of-attack range through which each model oscillated during the flight. In the following sections the experimental results are presented graphically and are compared with other available experimental data and theoretical estimates based on conical-flow theory for air (ref. 13) and the equations presented in reference 14 based on Newtonian theory. Enthalpy values of atmospheric flight were duplicated in the tests at Mach numbers of 11.5 and 19.5; at $M_\infty = 34.0$ the enthalpy was approximately 58 percent that of atmospheric flight at this Mach number. In the tests at Mach numbers 19.5 and 34, the heating rates were sufficiently high to cause ablation of the plastic models. These models survived the flights without significant change in shape. The effects of gas dissociation and surface ablation cannot be isolated and are implicit in the experimental results. Shadowgraphs, typical of those obtained in the present tests, are presented in figure 5 to show gross features of the flow fields, particularly the bow shock waves.

Drag Characteristics

The measured values of drag coefficient for both configurations are presented as a function of the root-mean-square resultant angle of attack in figure 6. As discussed earlier, this presentation is equivalent to a plot of C_D versus α, as would be obtained from conventional wind-tunnel tests. The experimental data show that the drag coefficients of both configurations increase with increasing angle of attack and are little affected by changes in Mach number from 11.5 to 34. The slightly higher drag coefficients obtained for both configurations at a Mach number of 34 may result from a 5- to 10-percent bias in the value of free-stream density used to compute the coefficients. The effect of angle of attack on the drag coefficients of both configurations is well predicted by Newtonian theory ($C_{p_{max}} = 2$).

Figure 7 presents the drag coefficients of both configurations at zero angle of attack as a function of Mach number. These data were obtained from straight-line extrapolations of the experimental data of figure 6, when plotted versus σ_{rms}^2. The resultant model velocities obtained in the present tests are also indicated in this figure. The present experimental data in figure 7 show essentially no change with Mach number and good agreement with the experimental

data of references 3, 4, and 6, which are also included in this figure.[1] The good agreement between the present value of C_D for the pointed cone at a Mach number of 19.5 (in air) and the value obtained in reference 6 for the same configuration at essentially the same Mach number in helium indicates that the combined effects of differences in the two tests, such as model ablation (the Teflon models used in the present tests at this Mach number ablated during flight, the model in the tests of reference 6 did not), enthalpy level of the tests, test gas, and Reynolds number, had little effect on the drag coefficient at zero angle of attack of this configuration. Conical-flow theory adequately predicts the drag coefficient of the pointed cone at zero angle of attack. The small increase in drag coefficient (approximately 8 percent) because of an increase in nose bluntness from $r_n/d = 0$ to $r_n/d = 0.20$ is overpredicted by Newtonian theory.

Static-Stability Characteristics

The experimental values of pitching-moment-curve slope, $C_{m_{\alpha_L}}$, based on the assumption of a linear restoring moment, are presented in figure 8 for both configurations versus the *maximum* resultant angle of attack, σ_m. In the event that the restoring moment is nonlinear with angle of attack, the stability results, unlike the drag results, are not correlated with σ_{rms}. They are instead presented as a function of σ_m, which is convenient for further analysis of the data by nonlinear methods. The data presented in figure 8 are for a moment reference center located at the center of volume of the particular configuration. It should be noted, however, that the difference between the center-of-gravity locations of the homogeneous configurations, as measured from the base, is only about 0.009 d (see fig. 2); hence, the correction to the static-stability data to provide comparison on the basis of a common center-of-gravity position would be small (approximately 4 percent). It should also be mentioned here that the stability data obtained at a Mach number of 11.5 were not corrected for the small change in center-of-gravity position due to the small shaft extending from the base of each model (see figs. 3 and 5) since this correction would increase the measured stability by less than 1 percent.

The data presented in figure 8 show that both configurations are statically stable at all Mach numbers and angles of attack of the investigation. In general, the data show that for an increase in Mach number from 11.5 to 34 the stability of the pointed cone increases slightly and that the stability of the blunted cone remains essentially constant. The static stability of both configurations is seen to decrease with increasing angle of attack. This variation of $C_{m_{\alpha_L}}$ with σ_m indicates the variation of pitching moment with angle of attack is not linear for either configuration and requires an appropriate method of nonlinear analysis. Theoretical estimates calculated at zero angle

[1]It should be noted that the blunted cone of reference 3 did not have exactly the same nose bluntness as that of the present blunted cone ($r_n/d = 0.167$ as compared to $r_n/d = 0.20$ for the present configuration); however, according to Newtonian theory the effect of this difference in nose bluntness on drag coefficient is negligible and, therefore, direct comparison between the two configurations is justified.

of attack using conical-flow theory and/or Newtonian theory agree with the experimental data (extrapolated to $\alpha = 0$) within about 10 percent. (Since the variation of C_{m_α} with "true" α is not known, this comparison between theory and experiment is valid only at zero angle of attack.)

There are several methods (refs. 15-19) of analyzing the observed pitching and yawing motions of a symmetrical body having a nonlinear pitching moment to obtain C_m as a function of α. The method of reference 19, developed under the assumption that the nonlinear moment can be described by an arbitrary power series of the resultant angle of attack, was used to analyze the data obtained in the present tests. This method was used according to the procedures described in the appendix of reference 5, and showed that the present nonlinear pitching moment for each Mach number could be closely approximated by the simplest of the moment representations tried, namely, $C_m = A\sigma + B\sigma^3$. (This case of a cubic pitching-moment representation is developed in ref. 17.)

The derived pitching-moment curves are shown in figure 9. These curves are considered valid only within the angle-of-attack range of the experimental data; therefore, they are terminated at the maxima obtained for each Mach number (see fig. 8). Examination of the experimental data shows, as expected, that for the angle-of-attack ranges of the data the stability of the pointed cone (fig. 9(a)) increases approximately 6 percent for an increase in Mach number from 11.5 to 19.5 and approximately 16 percent (±10 percent due to uncertainty in measurement of free-stream density of countercurrent air stream) for a further increase in Mach number to 34, and that the stability of the blunted cone (fig. 9(b)) is less affected by these changes in Mach number. The effect of angle of attack on pitching moment for both configurations is well predicted by Newtonian theory. The theoretical values of C_m are generally within about 10 percent of the experimental values for the angle-of-attack ranges of this investigation.

The initial stability of the configurations is compared in figure 10 with theoretical estimates calculated using conical-flow theory and/or Newtonian theory and with other available experimental data. The present experimental data show that the initial stability of both configurations at the high Mach numbers (M_∞ = 11.5 to 34) is very nearly the same as that measured at the lower Mach numbers (M_∞ = 4 to 8) in references 3 and 4. The excellent agreement between the present experimental data for the pointed cone at a Mach number of 19.5 (in air) and the data of reference 6 at essentially the same Mach number in helium (M_∞ = 20.3) indicates again that the different conditions of the two tests, that is, model-surface ablation, test gas, enthalpy level, and Reynolds numbers, had little effect on the data. The experimental data also show that the initial stability of the blunted cone is greater than that of the pointed cone by as much as 40 percent. This increase in initial stability for an increase in nose bluntness from $r_n/d = 0$ to $r_n/d = 0.20$ is, in general, underpredicted by Newtonian theory.

Dynamic-Stability Characteristics

The measured dynamic-stability parameter, ξ, for both configurations is presented in figure 11 as a function of the maximum resultant angle of

attack, σ_m. Negative values of ξ represent a convergent model motion (dynamic stability); positive values of ξ represent a divergent model motion (dynamic instability). The bars presented in figure 11 indicate the uncertainty in the measured values of ξ, at the values of σ_m shown, due to probable random errors of $\pm 0.5^\circ$ in the angle-of-attack measurements. As can be seen, the uncertainty in the values of ξ, obtained from the low-amplitude flights, is relatively large, since the error in ξ is proportional to the percentage error in amplitude which increases as the amplitude decreases. Also, as noted in the length of the bars shown in figure 11, the uncertainty in ξ is greater for the data obtained at a Mach number of 34 than at the two lower Mach numbers (M_∞ = 11.5 and 19.5), since the free-stream air density for the Mach number 34 tests is very low. The experimental data presented in figure 11 show that both configurations are dynamically stable at Mach numbers of 11.5 and 19.5 and that the dynamic stability remains constant, within the scatter of the data, for this increase in Mach number and for the angle-of-attack range investigated. These data at Mach numbers of 11.5 and 19.5 also show that the dynamic stability of both configurations is essentially the same; a reasonable average value of ξ is -3 and is approximately equivalent to a convergence of about 3 percent per cycle for conditions of the test. As the Mach number is increased further to 34, the results indicate large changes in the dynamic stability of both configurations and in opposite directions; the blunted cone becomes more dynamically stable and the pointed cone becomes dynamically unstable.[2] The dynamic instability of the pointed cone appears to be greatest at low amplitudes and a strong function of angle of attack.

These large changes in the dynamic stability of both configurations for an increase in Mach number from 19.5 to 34 were not expected, particularly so, since the drag and static-stability characteristics of both configurations showed no large changes for this increase in Mach number. These differences in the dynamic-stability results from Mach number 19.5 to 34 cannot be attributed to model damage during launch since, as stated earlier, the models used in these tests at Mach number 34 were of the same material (Teflon) and were launched at the same velocity as the models in the tests at a Mach number of 19.5. The reasons for these changes are not known; however, the principal differences between the tests at Mach numbers 19.5 and 34 (namely, the large increase in Mach number, the increased rates of ablation of the bodies produced by an increase of about a factor of 2 in convective heating, and the increased gas dissociation) can certainly contribute to producing these results. Concerning the possibility that the increased rates of ablation contributed to producing these changes, it is important to mention that some of the shadowgraphs showed evidence that ablated particles (indicated by the streaks, Mach waves, in the example shadowgraphs presented in fig. 5(c)) were present in the flow fields of almost all the models flying at a Mach number of 34, whereas the shadowgraphs of the models flying at a Mach number of 19.5 (see, e.g., fig. 5(b)) showed no evidence of such particles although these models also ablated during flight. It should be mentioned that these particles were observed in only a few of the shadowgraphs obtained for a particular flight,

[2]Because of premature firing of some of the observation stations, the motion histories obtained for flights 429 and 432 (see table I) were shorter and not well defined and were therefore less than adequate for measurement of dynamic stability.

usually those obtained at the latter stations (i.e., stations 9, 10, and 11), and were most visible in pictures that had a "schlieren effect." Unfortunately, further comparison of the flow field over the models at the different Mach numbers which may have provided some insight into the problem was not possible since these tests were conducted, of necessity, at low free-stream air densities where good flow-field visualization in the shadowgraphs is not easily attainable (see fig. 5). Another important difference is that the tests at Mach number 19.5 were conducted in still air, whereas the tests at Mach number 34 were conducted in a countercurrent air stream which, if irregularities were present, may have influenced the dynamic stability. However, it must be noted that the test conditions at Mach number 34 were identical for both configurations; that is, the same nominal 1.8 km/sec countercurrent air stream was employed in all the tests at this Mach number, so that any irregularities in the countercurrent flow should have influenced the dynamic-stability results of both configurations in the same manner. Hence, the difference between the results obtained for the pointed cone and the blunted cone indicates a real dependence of dynamic stability on nose geometry. Also the internal consistency of the results for each configuration indicates strongly that any random irregularities in the countercurrent air flow had little effect on the present results.

One other factor concerning the dynamic stability at Mach number 34 must be considered, namely, the variation of free-stream density with distance or time measured for each flight. The results have been adjusted as accurately as possible to remove this effect of the density gradient which, as stated previously, was from about 10 to 20 percent from beginning to end of all the flights of the models. The corrections were determined in the following manner: A motion was generated for each of the flights using the single-degree-of-freedom-motion equation together with the measured variation of density with distance, the value of $C_{m_{\alpha_L}}$ and initial values of σ and $\dot{\sigma}$ (obtained from analysis of the measured angular-orientation data by the method of reference 11), and an arbitrary "best estimate" of the value of ξ.[3] Discrete points (at very short intervals) of this generated motion were then taken as input data for the constant-density analysis using equation (2). The difference between the values of ξ, obtained from this analysis of the generated motion, and the input value of ξ, used to generate the motion initially, gave a correction for the effect of the density gradient.[4] This correction was applied to the value of ξ obtained originally from analysis by equation (2) of the measured angular-orientation data of a particular flight. Since the free-stream density decreased during the course of the model flight, these

---

[3]Determination of the required correction was found to be independent of the input value of ξ chosen. For example, input values of $\xi = +20, -20$, and 0 gave essentially the same value of the required correction for a particular flight.

[4]This analysis of the generated motion also gave a value of $C_{m_{\alpha_L}}$ which in all cases agreed with the input value within 1 percent and showed that a density gradient has little effect on the determination of C_{m_α} when an average value of ρ_∞ is used in the computations.

corrections to the data were negative (contributing dynamic stability) and for most of the flights, not very large; these corrections were less than $\Delta\xi = -3$ for all the flights with the exception of flights 449 and 639, which had corrections $\Delta\xi$ of -10 and -7, respectively, because of greater density gradients.[5] It should be stated again, however, that the results at this Mach number (M = 34) are still subject to ±10 percent error owing to the initial uncertainty in the measurement of free-stream density (see discussion under Description of Tests). Corrections in ξ due to the measured density gradient of each flight were also computed using Friedrich and Dore's expression for amplitude change due to dynamic pressure variation (see ref. 20)

$$\frac{\alpha_{max}}{\alpha_{max_i}} = \left(\frac{q_{\infty_i}}{q_{\infty_f}}\right)^{1/4} \tag{7}$$

When this amplitude change is substituted in the expression

$$\frac{\alpha_{max}}{\alpha_{max_i}} = e^{\frac{\rho_\infty A}{4m}\Delta x\,\Delta\xi} \tag{8}$$

an increment in ξ, designated $\Delta\xi$, is calculated which represents the correction to be applied to the apparent value of ξ indicated by the divergence, or convergence, of the angular motion. Different values of $\Delta\xi$ will be obtained from equations (7) and (8) for a given constant density gradient as the length of the distance interval Δx is varied, because of the 1/4-power dependence of $\alpha_{max}/\alpha_{max_i}$ on $q_{\infty_i}/q_{\infty_f}$, but as $\Delta x \to 0$, $\Delta\xi \to$ constant, $(dq_\infty/dx)/(\rho_\infty A/m)q_{\infty_f}$. The variation in $\Delta\xi$ with Δx for large variations in q_∞ is proper, since the effect is nonlinear. This relatively simple method gave values for the corrections which were within ±2 of the values obtained by the previously described procedure. However, it is believed that the final values of ξ were more precise when the corrections were computed by the previously described procedure because the values of ξ to be adjusted were determined by use of the method of reference 11. This method is not rigorously applicable to cases of variable-density flight (but is necessary in establishing the best fitting continuous angular motion), and any errors introduced in these values of ξ by inapplicability of the equation should be canceled by use of the same method (ref. 11) in computing the corrections.

It should be mentioned that dynamic stability is not of critical importance during the high-speed (early) portion of ballistic entries since the rapid increase in atmospheric density strongly damps vehicle oscillations. However, for shallow-angle entries such as will be used for manned vehicles entering planetary atmospheres, the flights will be at essentially constant altitude in which case the dynamic stability of the vehicle at these very high speeds is of great importance. Also, if the dynamic instability measured for

[5]It is important to mention that the density variation measured for flight 623 increased during the model flight; therefore the correction to the value of ξ obtained for this flight was positive ($\xi = +0.8$).

the pointed cone at a Mach number of 34 is in fact caused by increased rates of ablation, then this effect might possibly occur at lower speeds which would warrant further study in these areas.

Included in figure 11(b) are two values of ξ obtained at a Mach number of 4 for a cone having a nose bluntness of $r_n/d = 0.167$ in reference 3. These values are seen to lie within the scatter of the present experimental data for the blunted cone obtained at similar low angles of attack.

Values of the dynamic-stability parameter, ξ, at zero angle of attack estimated for both configurations using Newtonian theory and equation (5) are also presented in figure 11.[6] Comparison shows that the theoretical estimates agree with the experimental data obtained for both configurations at Mach numbers of 11.5 and 19.5. Although the theoretical estimates are shown only at zero angle of attack, it is noted that Newtonian theory predicts essentially constant dynamic stability for both configurations for the entire angle-of-attack range covered by the present experimental results.

CONCLUSIONS

An experimental study conducted in air at Mach numbers of 11.5, 19.5, and 34 of a pointed and a blunted 30° half-angle cone has led to the following conclusions.

1. Both configurations were statically stable, for center-of-gravity positions located at the models' centers of volume, at all Mach numbers and angles of attack of the investigation. The static stability of the pointed cone increased with increasing Mach number. The static stability of the blunted cone was essentially invariant with Mach number and greater than that of the pointed cone by as much as 40 percent. The static stability of both configurations decreased with increasing angle of attack.

2. The nonlinear variation of pitching moment with angle of attack for both configurations was closely approximated by a cubic polynomial at $\alpha < 25°$.

3. Both configurations were dynamically stable at Mach numbers of 11.5 and 19.5 for unpowered flight at constant altitude and exhibited pitching motions which converged at the rate of about 3 percent per cycle. At a Mach number of 34 the blunted cone exhibited increased dynamic stability, and the pointed cone became dynamically unstable. The dynamic instability of the pointed cone became less severe with increasing amplitude of oscillation.

---

[6]Newtonian theory gives values of C_{m_q} which were in excellent agreement with the values of $C_{m_q} + C_{m_{\dot{\alpha}}}$ computed using the present experimental values of ξ, C_D, and the values of C_{I_α} predicted by Newtonian theory in equation (5).

4. The drag coefficient of both configurations increased with increasing angle of attack and remained essentially constant with increasing Mach number. The drag of the blunted cone was approximately 8 percent greater than that of the pointed cone.

5. The static-stability and drag characteristics of both configurations were predicted by Newtonian theory, and for the pointed cone, by conical-flow theory, usually within about 10 percent. The dynamic stability of both configurations, calculated using Newtonian theory, was in agreement with the mean level of the experimental results at Mach numbers of 11.5 and 19.5.

Ames Research Center
National Aeronautics and Space Administration
Moffett Field, Calif., Nov. 22, 1965

REFERENCES

1. Allen, H. Julian; Seiff, Alvin; and Winovich, Warren: Aerodynamic Heating of Conical Entry Vehicles at Speeds in Excess of Earth Parabolic Speed. NASA TR R-185, 1963.

2. Demele, Fred A.: A Study of the Convective and Radiative Heating of Shapes Entering the Atmospheres of Venus and Mars at Superorbital Speeds. NASA TN D-2064, 1963.

3. Seiff, Alvin; Sommer, Simon C.; and Canning, Thomas N.: Some Experiments at High Supersonic Speeds on the Aerodynamic and Boundary-Layer Transition Characteristics of High-Drag Bodies of Revolution. NASA RM A56I05, 1957.

4. Penland, Jim A.: A Study of the Stability and Location of the Center of Pressure on Sharp, Right Circular Cones at Hypersonic Speeds. NASA TN D-2283, 1964.

5. Intrieri, Peter F.: A Study of the Stability and Drag at Mach Numbers From 4.5 to 13.5 of a Conical Venus-Entry Body. NASA TN D-2827, 1965.

6. Maddalon, Dal V.: Aerodynamic Characteristics of the Sharp Right Circular Cone at Mach 20.3 and Angles of Attack to 110° in Helium. NASA TN D-3201, 1966.

7. Seiff, Alvin: Ames Hypervelocity Free-Flight Research. Astronaut. Aerospace Eng., vol. 1, no. 11, Dec. 1963, pp. 16-23.

8. Curtis, John S.: An Accelerated Reservoir Light-Gas Gun. NASA TN D-1144, 1962.

9. Seiff, Alvin: A New Method for Computing Drag Coefficients From Ballistic Range Data. J. Aero. Sci., vol. 25, no. 2, 1958, pp. 133-134.

10. Seiff, Alvin; and Wilkins, Max E.: Experimental Investigation of a Hypersonic Glider Configuration at a Mach Number of 6 and at Full-Scale Reynolds Numbers. NASA TN D-341, 1961.

11. Nicolaides, John D.: On the Free-Flight Motion of Missiles Having Slight Configurational Asymmetries. BRL Rep. 858, Aberdeen Proving Ground, Md., 1953.

12. Allen, H. Julian: Motion of a Ballistic Missile Angularly Misaligned With the Flight Path Upon Entering the Atmosphere, and Its Effect Upon Aerodynamic Heating, Aerodynamic Loads, and Miss Distance. NACA RM A56F15, 1956.

13. Staff of the Computing Section (under the direction of Zdeněk Kopal): Table of Supersonic Flow Around Yawing Cones. Tech. Rep. 3, Center of Analysis, M. I. T., Cambridge, 1947.

14. Margolis, Kenneth: Theoretical Evaluation of the Pressures, Forces, and Moments at Hypersonic Speeds Acting on Arbitrary Bodies of Revolution Undergoing Separate and Combined Angle-of-Attack and Pitching Motions. NASA TN D-652, 1961.

15. Kryloff, N. M.; and Bogoliuboff, N. N. (Solomon Lefschetz, transl.): Introduction to Non-Linear Mechanics. Annals of Mathematics Studies, no. 11, Princeton Univ. Press, Princeton, N. J., 1943.

16. Murphy, Charles H.: The Measurements of Non-Linear Forces and Moments by Means of Free-Flight Tests. BRL Rep. 974, Aberdeen Proving Ground, Md., 1956.

17. Rasmussen, Maurice L.: Determination of Nonlinear Pitching-Moment Characteristics of Axially Symmetric Models From Free-Flight Data. NASA TN D-144, 1960.

18. Kirk, Donn B.: A Method for Obtaining the Nonlinear Aerodynamic Stability Characteristics of Bodies of Revolution From Free-Flight Tests. NASA TN D-780, 1961.

19. Rasmussen, Maurice L.; and Kirk, Donn B.: On the Pitching and Yawing Motion of a Spinning Symmetric Missile Governed by an Arbitrary Nonlinear Restoring Moment. NASA TN D-2135, 1964.

20. Friedrich, Hans R.; and Dore, Frank J.: The Dynamic Motion of a Missile Descending Through the Atmosphere. J. Aero. Sci., vol. 22, no. 9, Sept. 1955, pp. 628-632, 638.

TABLE I.- TEST CONDITIONS AND DATA

(a) Pointed cone

Flight	M_∞	V_∞, km/sec	Re, million	C_D	$C_{m_{\alpha_L}}$	ξ	σ_m, deg	σ_o, deg	σ_{rms}, deg	d, cm	$\frac{x_{cg}}{d}$	m, g	$I_y \times 10^3$, kg-m^2	$\left(\frac{d}{k}\right)^2$
Nominal Mach number = 11.5, V_a = 0														
821	11.75	4.047	0.082	0.665	-0.161	-4.015	20.81	0.62	14.73	1.017	0.216	0.6851	4.498	15.77
822	11.95	4.128	.089	.608	-.157	-.883	16.59	2.39	11.95	1.015	↓	.6861	↓	15.71
823	11.76	4.065	.081	.812	-.117	-3.519	43.44	.96	29.18	1.019		.6821		15.76
832	11.79	4.080	.081	.641	-.156	-3.282	19.69	.19	14.07	1.018		.6871		15.83
833	10.46	3.616	.078	.561	-.160	---	2.49	.16	1.68	1.017		.6821		15.67
834	11.94	4.123	.079	.673	-.140	-3.252	27.80	1.34	18.89	1.015		.6868		15.72
835	11.29	3.900	.068	.580	-.160	-2.789	13.53	.04	9.54	1.017		.6803		15.65
836	11.41	3.926	.076	.581	-.159	-3.973	13.44	.21	9.57	1.015		.6843		15.70
841	11.40	3.934	.071	.580	-.155	-8.892	10.12	.89	7.13	1.016		.6810		16.62
843	11.42	3.932	.074	.626	-.159	-3.149	18.82	3.45	13.58	1.017		.6853		15.75
844	11.38	3.906	.069	.587	-.165	-6.656	11.03	1.21	7.63	1.015		.6817		15.62
Nominal Mach number = 19.5, V_a = 0														
924	19.45	6.724	.121	.516	-.174	-6.225	4.69	1.14	3.23	1.026	.216	.5135	3.461	15.63
925	19.62	6.774	.117	.523	-.178	-1.662	5.56	.29	3.97	1.016	↓	.5078	↓	15.13
926	19.59	6.729	.123	.508	-.172	-9.801	4.92	.06	3.31	1.028		.5156		15.34
927	19.50	6.757	.119	.536	-.170	-13.451	4.79	.26	3.19	1.025		.5196		15.78
928	19.40	6.734	.117	.538	-.183	-8.504	5.82	1.97	4.14	1.023		.5141		15.60
929	19.45	6.751	.116	.539	-.164	4.863	7.55	2.52	5.53	1.028		.5235		15.99
930	19.19	6.632	.115	.651	-.153	-4.943	25.18	2.27	17.31	1.025		.5189		15.77
931	19.21	6.639	.115	.543	-.163	-2.100	10.22	5.90	8.36	1.024		.5217		15.82
936	18.74	6.528	.115	.567	-.177	-1.382	14.65	.80	10.51	1.021		.5216		15.71
937	19.32	6.707	.114	.569	-.171	-6.297	12.87	3.21	9.00	1.018		.5239		15.68
Nominal Mach number = 34, V_a = 1.8 km/sec														
623	33.41	8.412	.171	.593	-.190	-7.414	20.44	1.11	12.40	1.016	.216	.5118	3.461	15.24
627	34.34	8.595	.164	.559	-.200	10.832	13.68	2.73	8.57	1.017	↓	.5207	↓	15.58
629	34.22	8.594	.169	.607	-.206	16.647	12.27	.88	7.98	1.018		.5281		15.76
631	34.60	8.643	.167	.561	-.196	37.386	7.55	1.99	4.78	1.018		.5266		15.78
633	35.06	8.637	.166	.714	-.189	5.237	21.70	3.50	15.36	1.017		.5294		15.84
635	33.97	8.534	.159	.618	-.177	7.920	18.95	.61	12.64	1.014		.5285		15.72

(b) Blunted cone

Flight	M_∞	V_∞, km/sec	Re, million	C_D	$C_{m_{\alpha_L}}$	ξ	σ_m, deg	σ_o, deg	σ_{rms}, deg	d, cm	$\frac{x_{cg}}{d}$	m, g	$I_y \times 10^3$, kg-m^2	$\left(\frac{d}{k}\right)^2$
Nominal Mach number = 11.5, V_a = 0														
824	12.00	4.143	.072	.673	-.205	-.848	21.99	.73	15.11	1.015	.207	.6736	4.231	16.41
826	11.41	3.936	.075	.580	-.235	1.611	7.91	1.19	5.78	1.017	↓	.6690	↓	16.35
827	10.97	3.780	.069	.608	-.225	-1.953	13.49	.44	9.33	1.019		.6640		16.27
831	11.27	3.900	.069	.635	-.243	-3.735	11.33	.29	8.07	1.016		.6732		16.43
838	12.26	4.236	.075	.577	-.225	-3.644	11.99	.12	8.30	1.020		.6640		16.33
839	11.26	3.897	.072	.593	-.212	-2.026	14.53	.84	9.89	1.016		.6732		16.42
840	11.18	3.863	.067	.640	-.218	-2.543	18.73	.83	12.87	1.013		.6572		15.96
842	11.48	3.953	.073	.722	-.169	-.223	31.51	.67	22.21	1.016		.6749		16.46
Nominal Mach number = 19.5, V_a = 0														
920	19.07	6.550	.115	.550	-.207	-12.32	4.62	.72	2.34	1.015	.207	.4986	3.255	15.79
921	19.63	6.797	.116	.572	-.228	-.251	2.95	.41	1.89	1.018	↓	.5055	↓	16.12
922	19.69	6.830	.115	.561	-.210	-8.573	4.31	.14	2.31	1.015		.4969		15.73
923	19.40	6.728	.117	.577	-.216	.423	3.44	.19	2.14	1.026		.5064		16.38
932	19.58	6.779	.122	.675	-.201	-2.773	24.29	.24	16.41	1.026		.5007		16.21
933	19.63	6.755	.125	.597	-.228	-5.689	11.35	.52	7.41	1.021		.5018		16.10
934	19.49	6.779	.120	.628	-.232	-.915	16.07	1.72	10.82	1.022		.4937		15.84
935	19.17	6.709	.115	.598	-.231	-3.380	10.08	1.05	6.82	1.019		.4952		15.80
938	19.37	6.724	.115	.589	-.229	-4.755	10.92	.85	6.96	1.021		.5059		16.22
Nominal Mach number = 34, V_a = 1.8 km/sec														
429	32.81	8.291	.159	.692	-.204	---	22.15	3.08	15.74	1.019	.207	.5073	3.255	16.20
432	33.95	8.402	.182	.676	-.219	---	20.47	2.21	13.69	1.020	↓	.5038	↓	16.10
436	36.00	8.624	.174	.640	-.237	-19.505	14.29	.36	10.07	1.017		.5011		15.94
449	33.00	8.427	.143	.607	-.244	-21.226	5.67	.27	4.00	1.024		.5064		16.31
637	34.73	8.818	.167	.761	-.172	-12.932	34.37	6.04	24.24	1.028		.5154		16.71
639	35.05	8.711	.164	.653	-.235	-21.528	14.48	.42	9.93	1.018		.5142		16.38

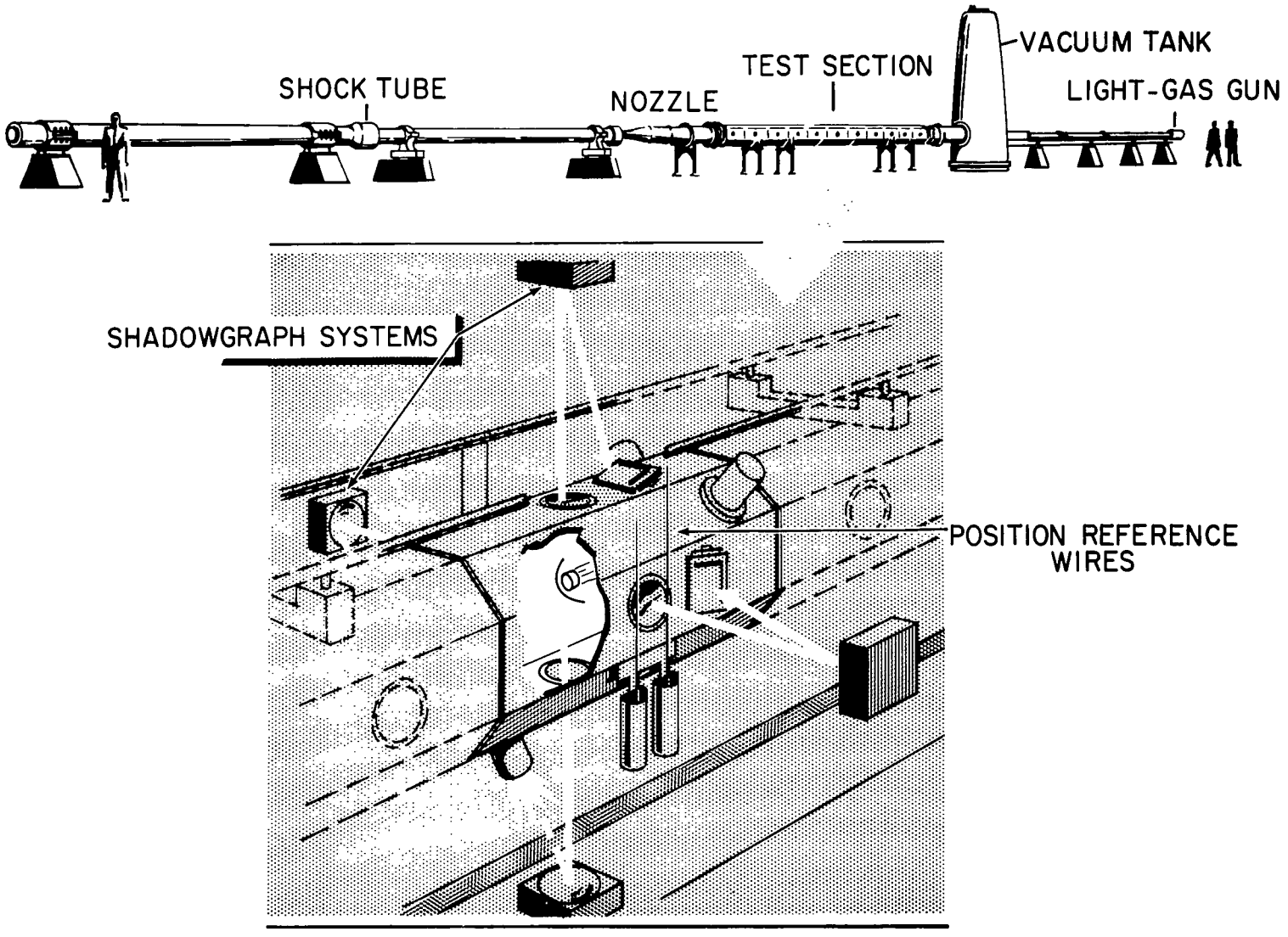

Figure 1.- Schematic drawing of Prototype Hypervelocity Free-Flight Facility.

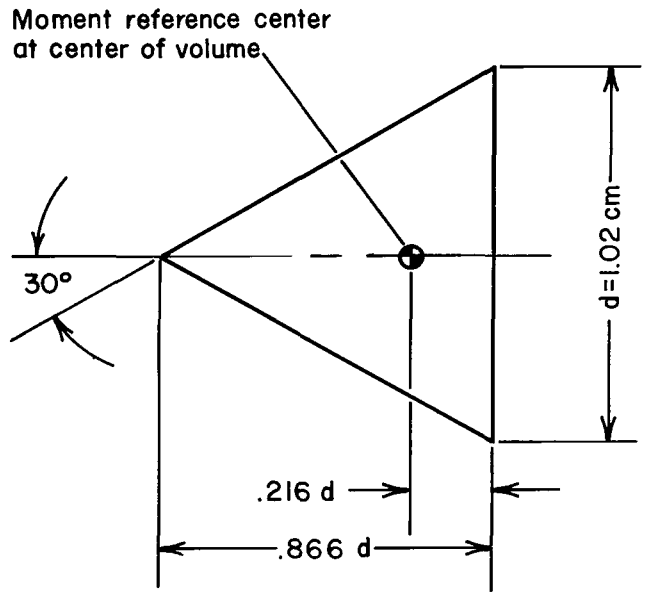

(a) Pointed cone

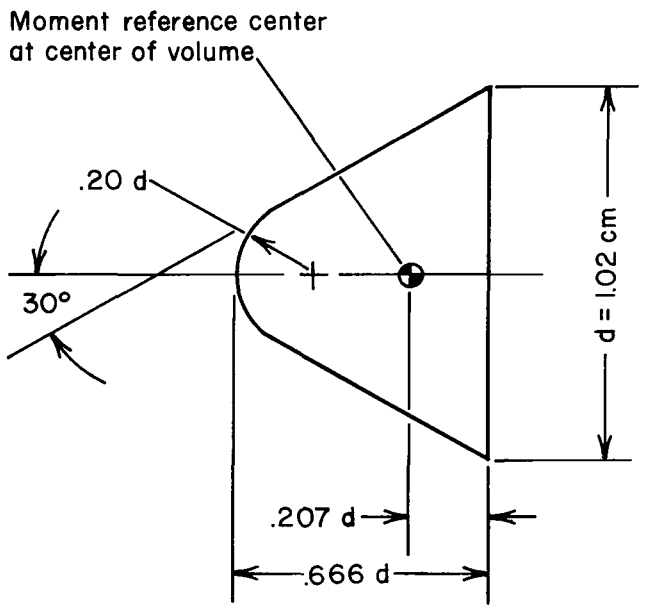

(b) Blunted cone

Figure 2.- Sketch of models showing nominal dimensions.

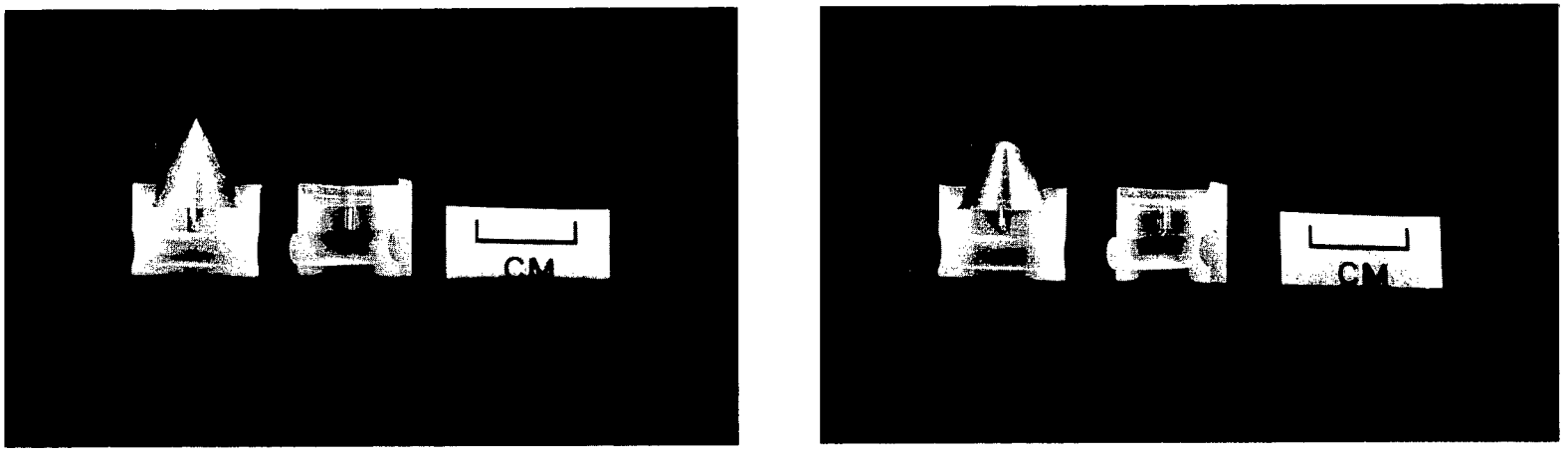

(a) Aluminum models with sabots

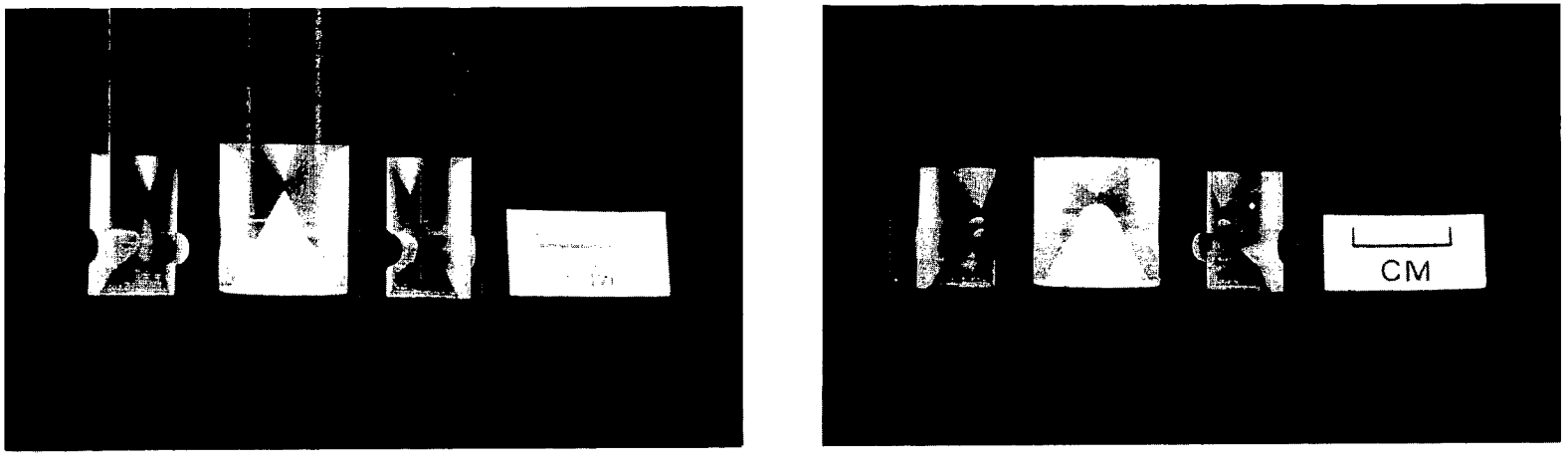

(b) Teflon models with sabots

Figure 3.- Photographs of models and sabots.

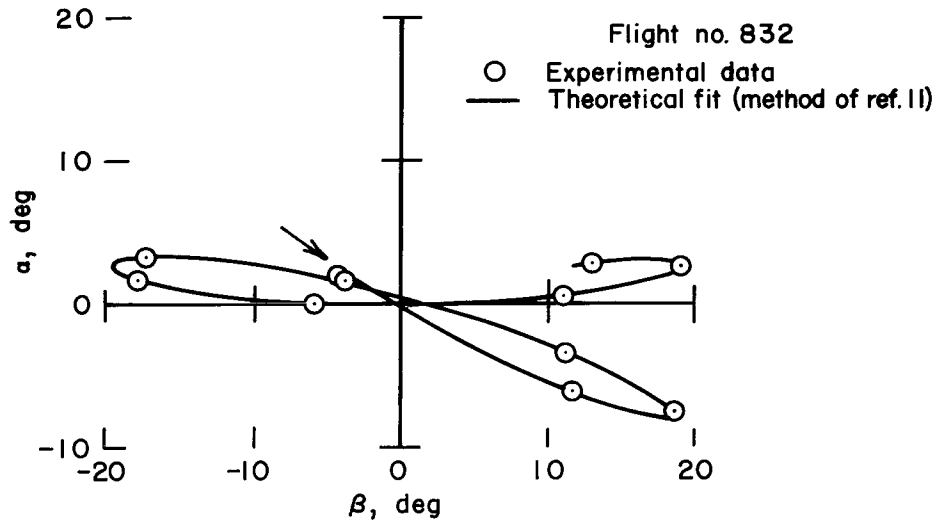

(a) M_∞ = 11.5 (Pointed cone)

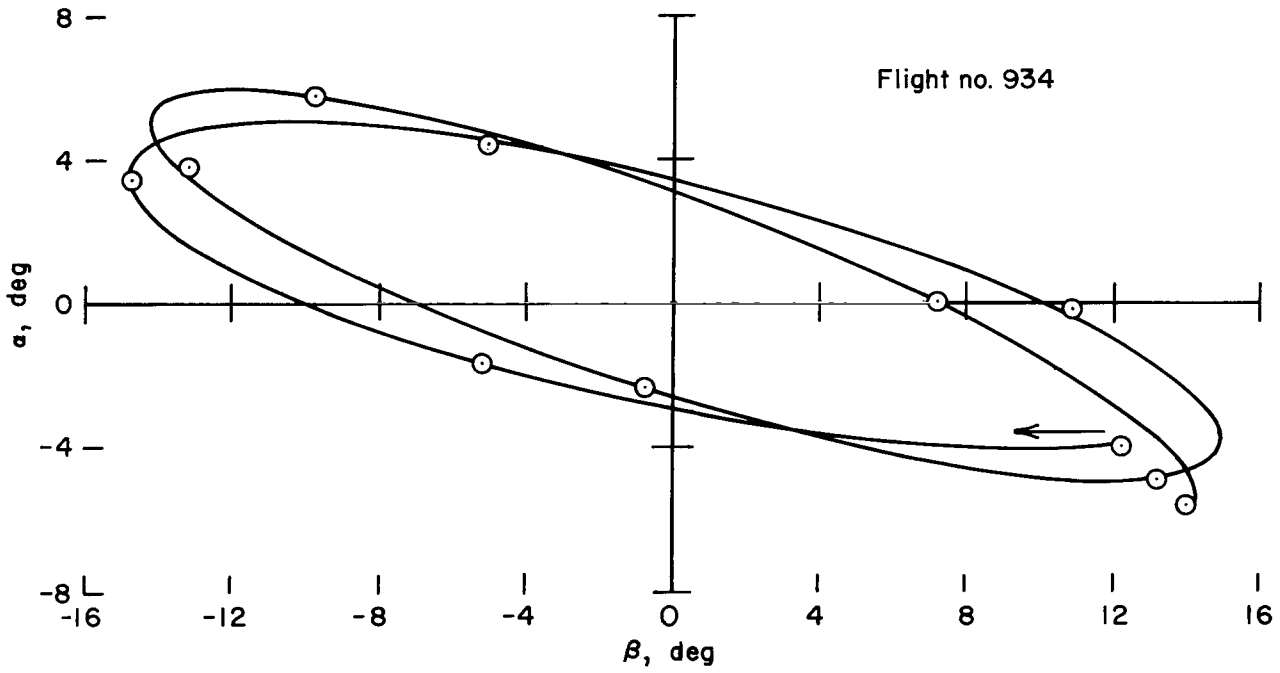

(b) M_∞ = 19.5 (Blunted cone)

Figure 4.- Typical pitching and yawing motions produced by the models.

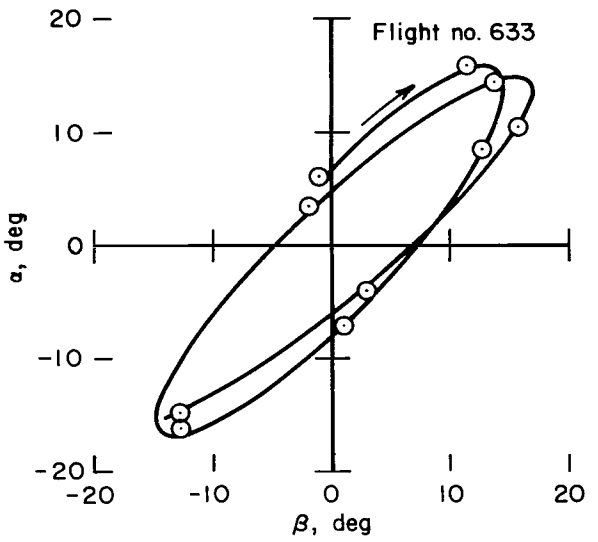

(c) $M_\infty = 34$ (Pointed cone)

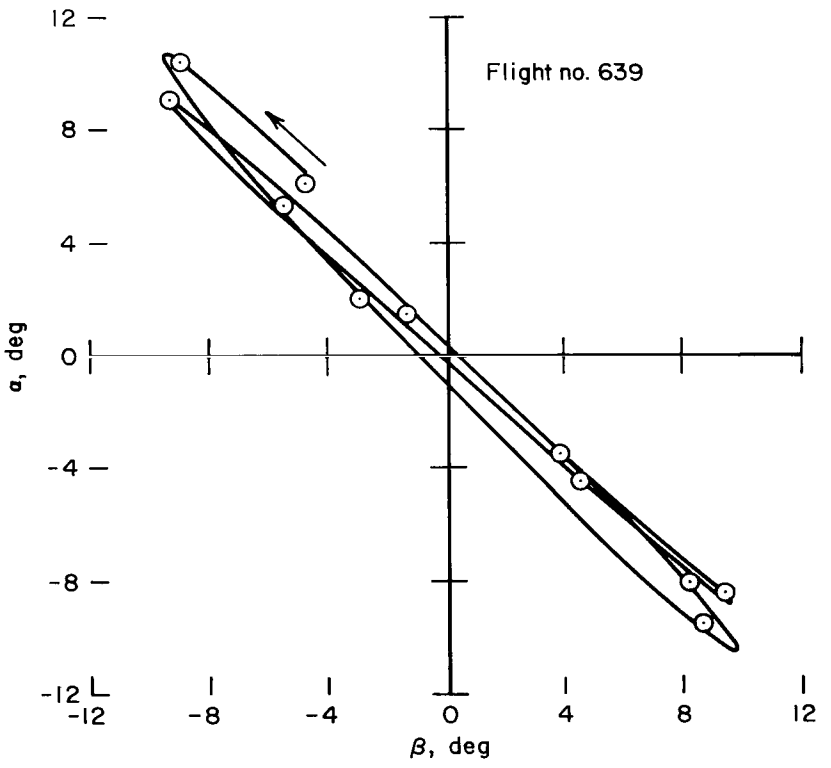

(d) $M_\infty = 34$ (Blunted cone)

Figure 4.- Concluded.

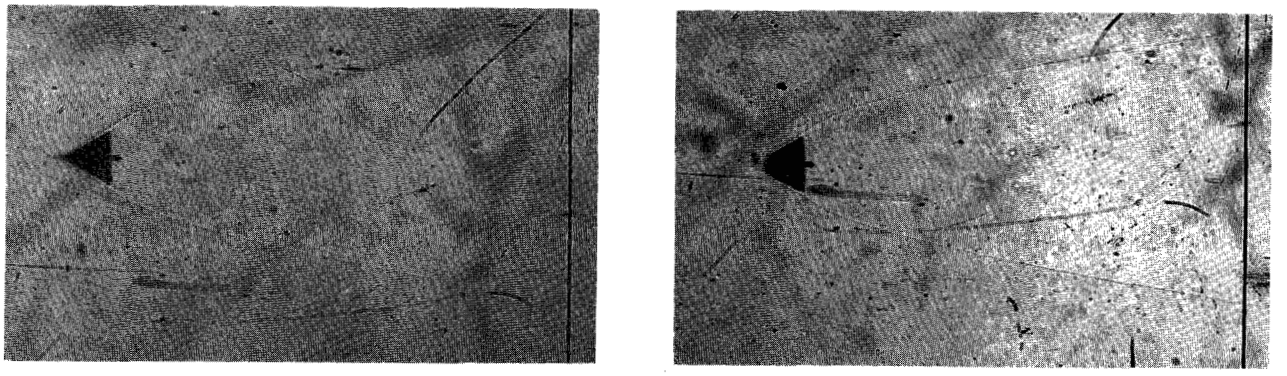

(a) M_∞= 11.5; V_∞= 4 km/sec

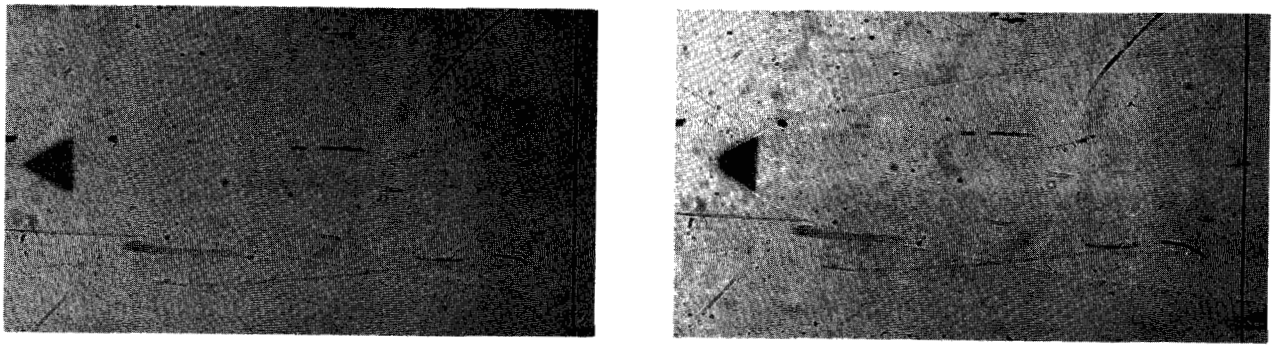

(b) M_∞= 19.5; V_∞= 6.7 km/sec

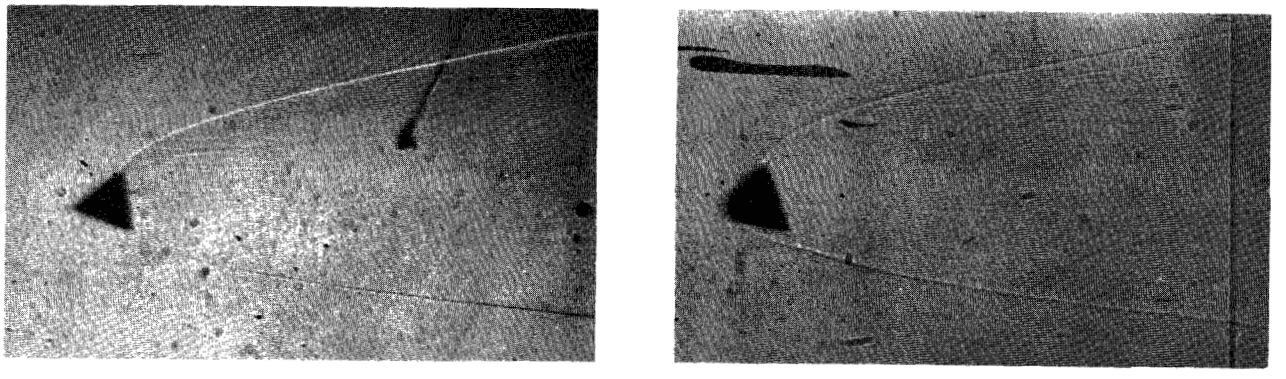

(c) M_∞= 34; V_∞= 8.5 km/sec

Figure 5.- Shadowgraphs of models in flight.

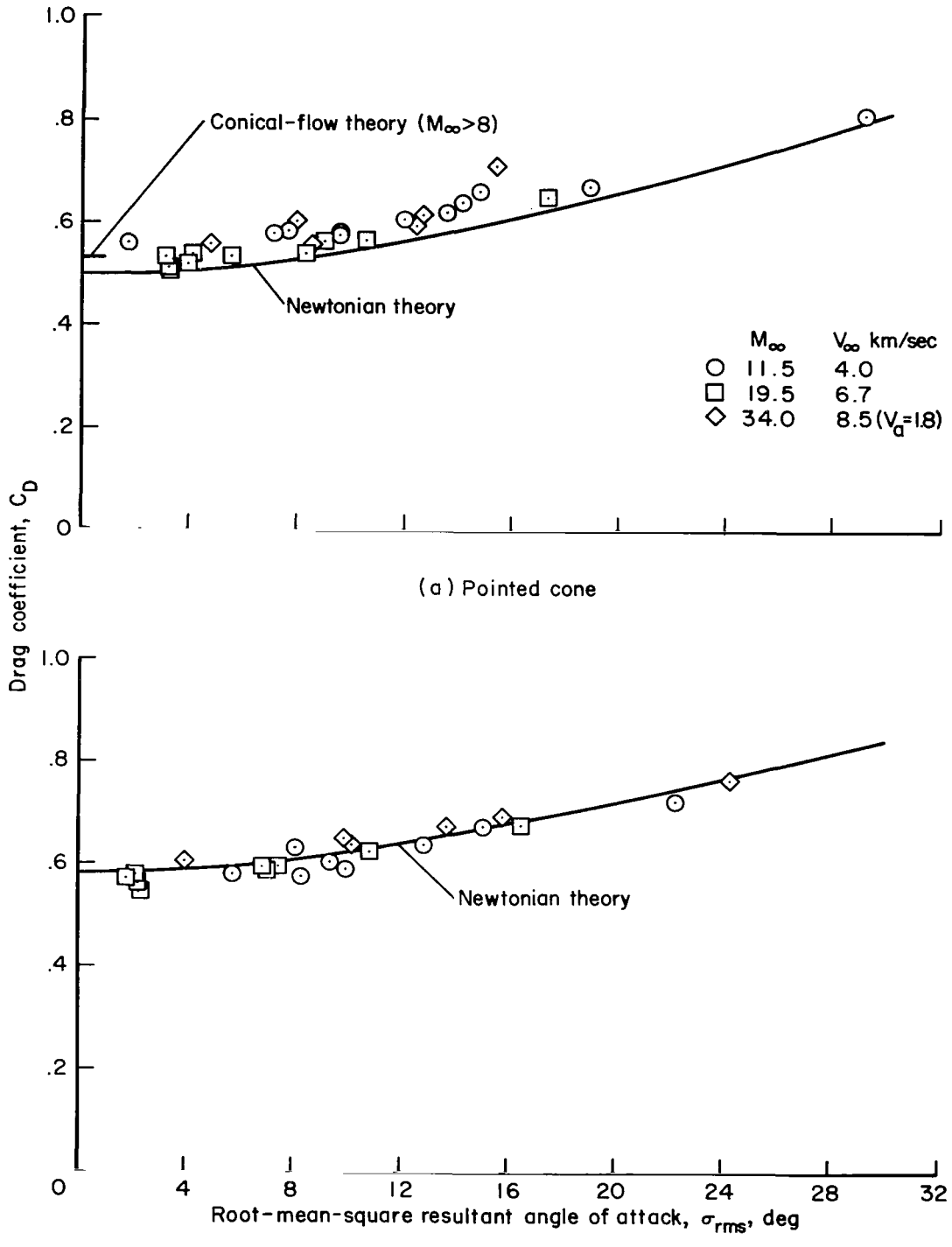

Figure 6.- Variation of drag coefficient with angle of attack.

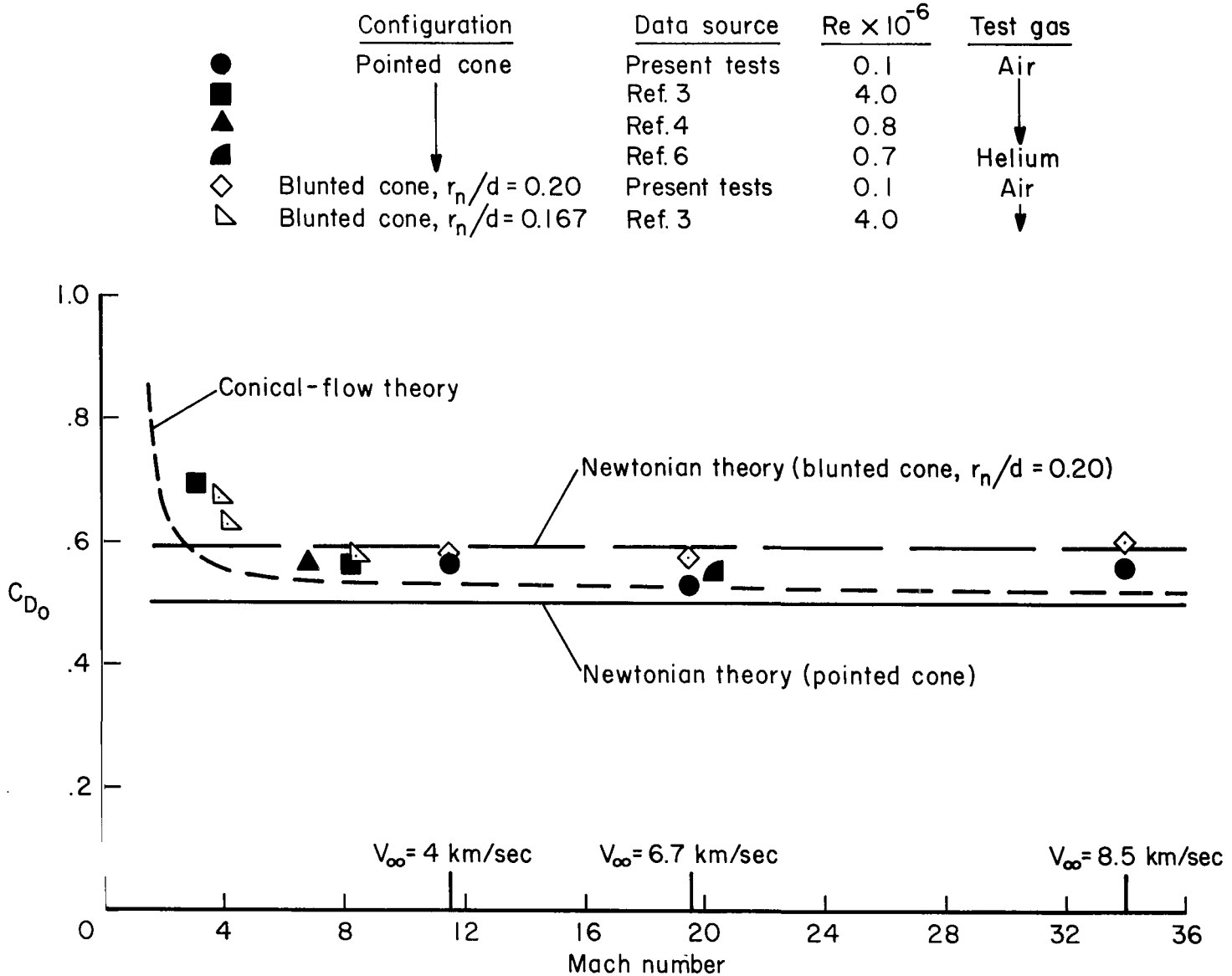

Figure 7.- Effect of Mach number and nose blunting on drag coefficient at $\sigma = 0^{\circ}$.

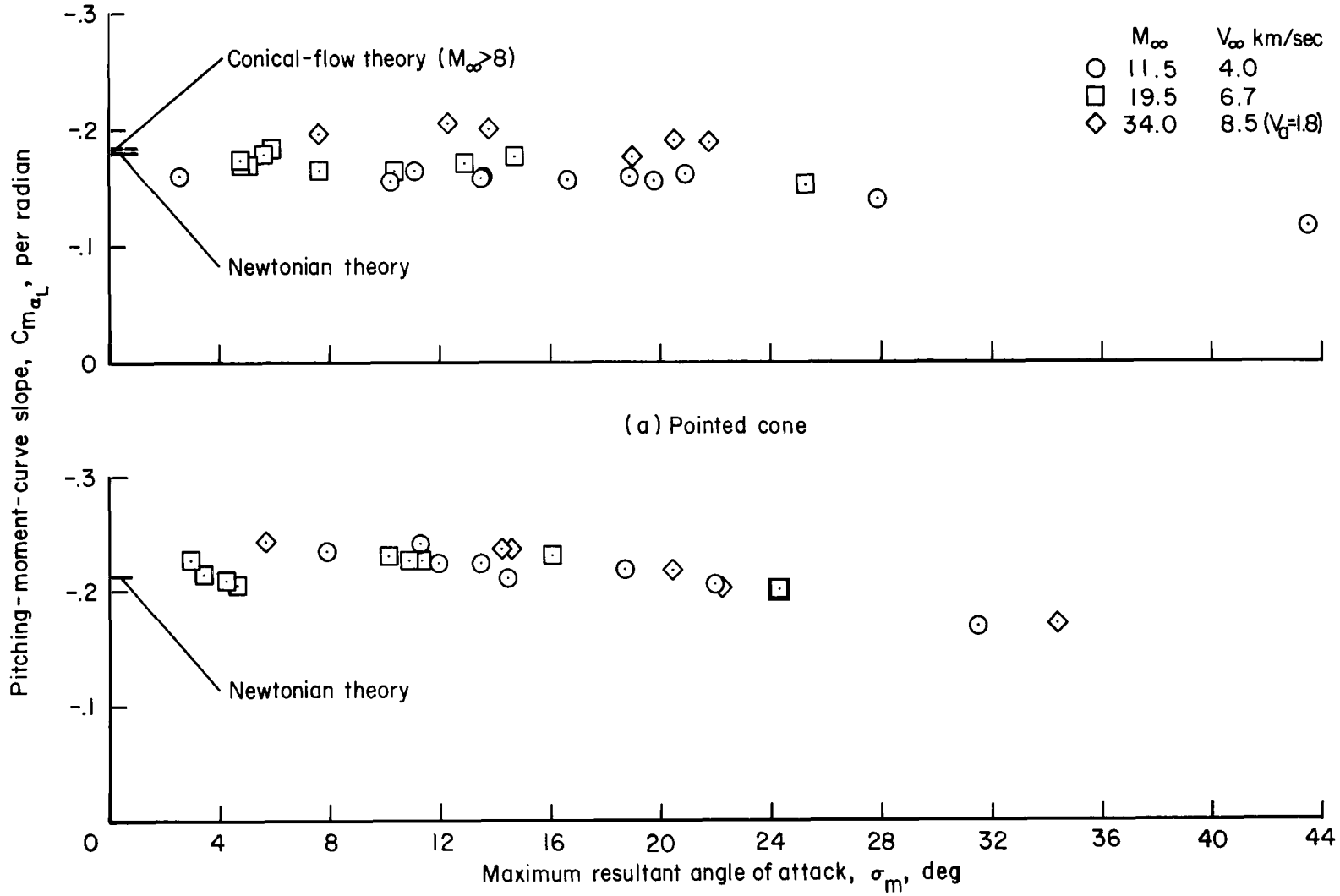

Figure 8.- Variation of experimental static-stability data with angle of attack (center of gravity at center of volume).

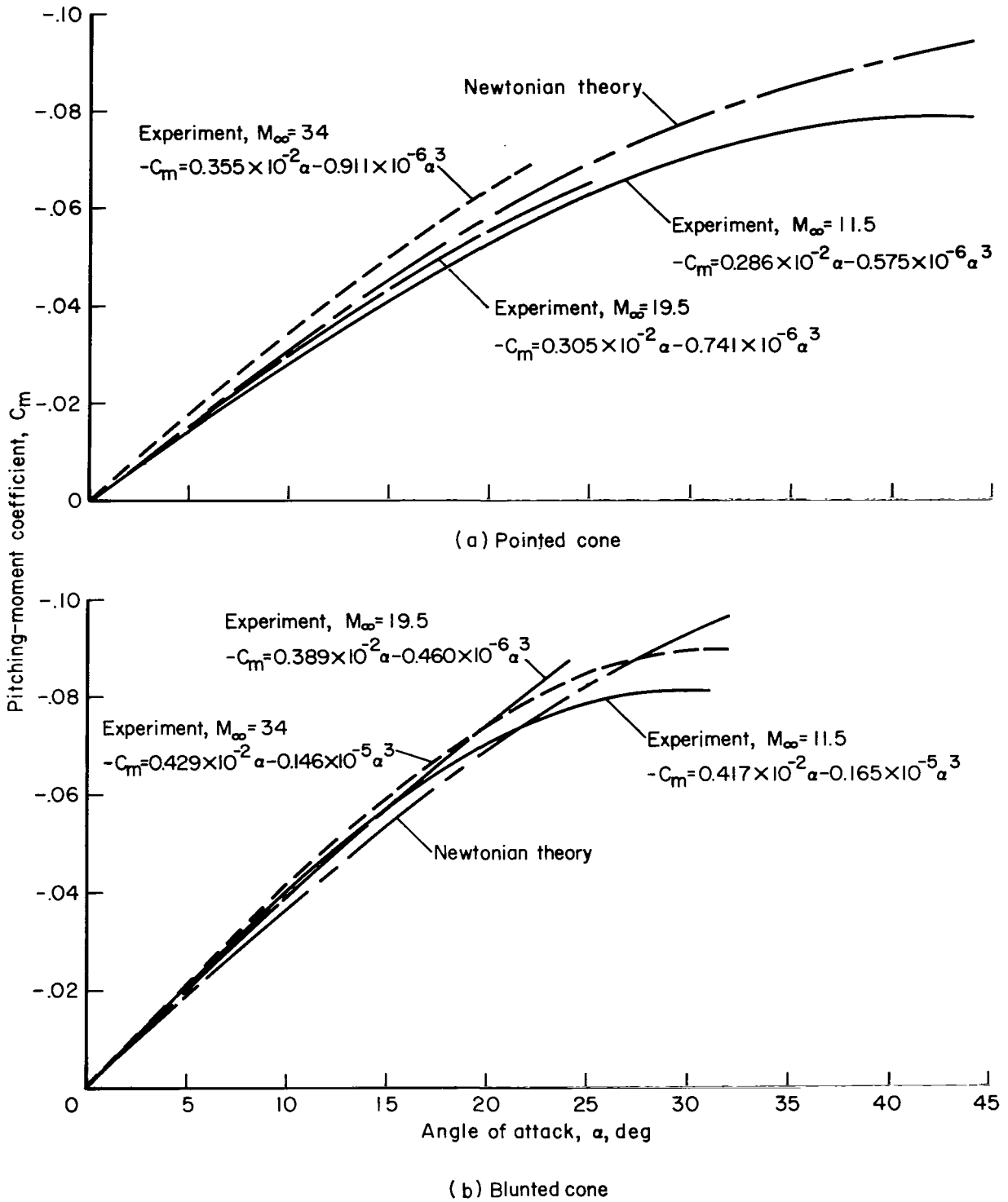

Figure 9.- Comparison of experimental pitching-moment coefficient with theory (center of gravity at center of volume).

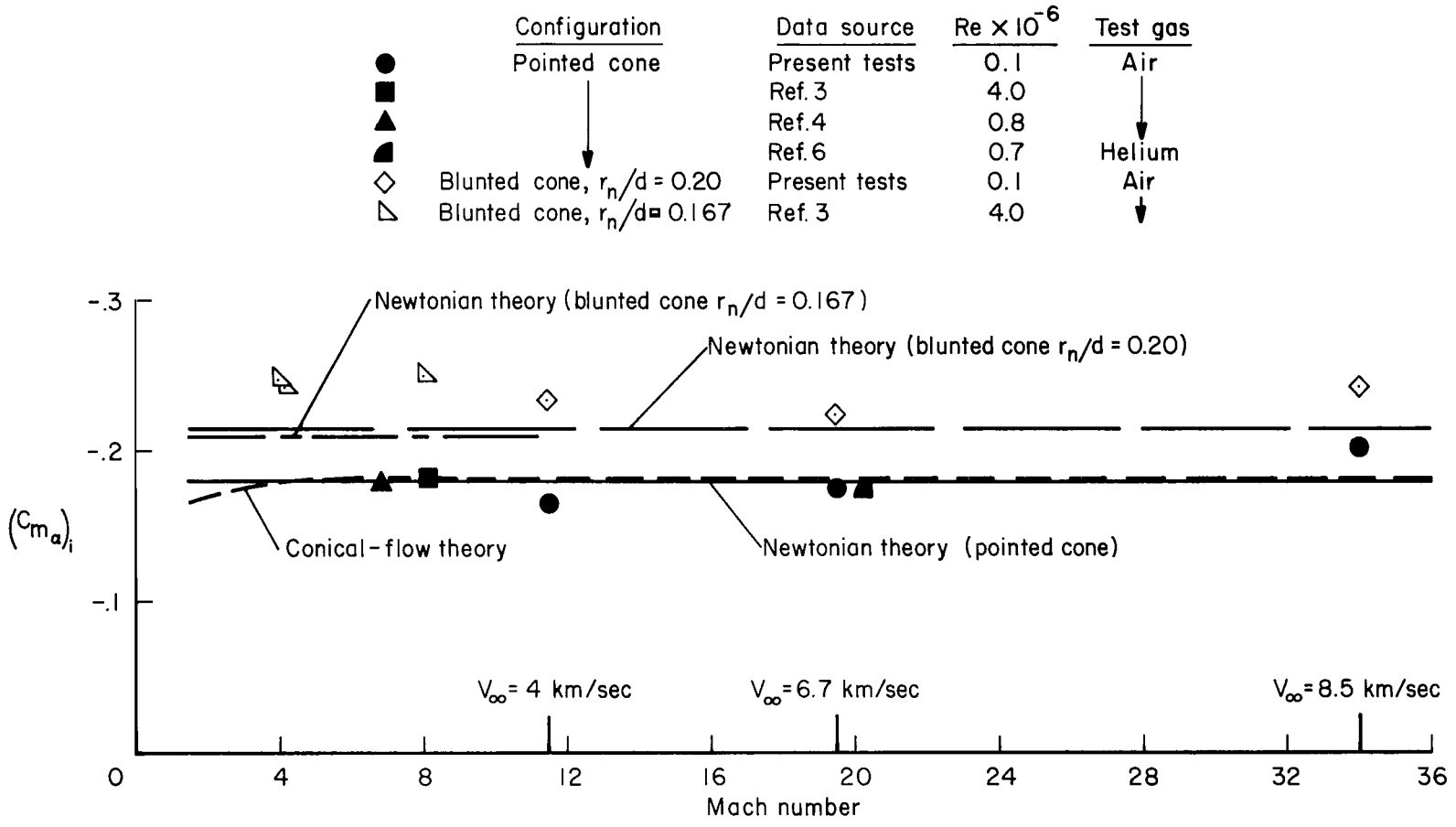

Figure 10.- Effect of Mach number and nose blunting on initial static stability (center of gravity at center of volume).

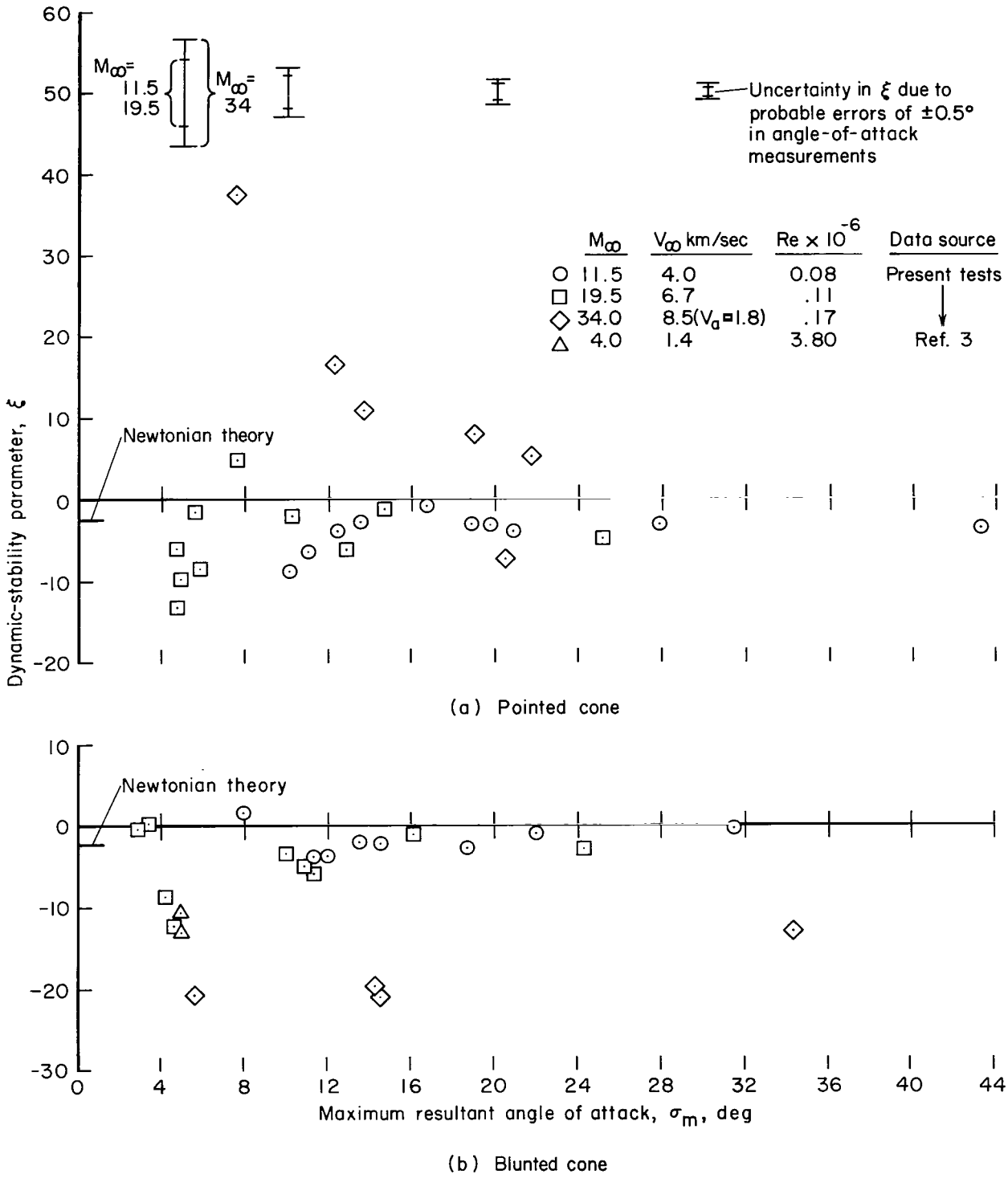

Figure 11.- Dynamic-stability results.

"The aeronautical and space activities of the United States shall be conducted so as to contribute . . . to the expansion of human knowledge of phenomena in the atmosphere and space. The Administration shall provide for the widest practicable and appropriate dissemination of information concerning its activities and the results thereof."

—NATIONAL AERONAUTICS AND SPACE ACT OF 1958

NASA SCIENTIFIC AND TECHNICAL PUBLICATIONS

TECHNICAL REPORTS: Scientific and technical information considered important, complete, and a lasting contribution to existing knowledge.

TECHNICAL NOTES: Information less broad in scope but nevertheless of importance as a contribution to existing knowledge.

TECHNICAL MEMORANDUMS: Information receiving limited distribution because of preliminary data, security classification, or other reasons.

CONTRACTOR REPORTS: Technical information generated in connection with a NASA contract or grant and released under NASA auspices.

TECHNICAL TRANSLATIONS: Information published in a foreign language considered to merit NASA distribution in English.

TECHNICAL REPRINTS: Information derived from NASA activities and initially published in the form of journal articles.

SPECIAL PUBLICATIONS: Information derived from or of value to NASA activities but not necessarily reporting the results of individual NASA-programmed scientific efforts. Publications include conference proceedings, monographs, data compilations, handbooks, sourcebooks, and special bibliographies.

Details on the availability of these publications may be obtained from:

SCIENTIFIC AND TECHNICAL INFORMATION DIVISION

NATIONAL AERONAUTICS AND SPACE ADMINISTRATION

Washington, D.C. 20546